VOL. 15, NO. 23, DECEMBER 2020 ISSN 1819-6608
ARPN Journal of Engineering and Applied Sciences

www.arpnjournals.com

DYNAMIC BEHAVIOUR OF STEEL ECCENTRICALLY BRACED FRAMES HAVING MOMENT-SHEAR LINK

Alireza Bahrami[1,2] and Mahmood Heidari[2]
[1]Department of Building Engineering, Energy Systems, and Sustainability Science, Faculty of Engineering and Sustainable Development, University of Gävle, 801 76 Gävle, Sweden
[2]Department of Civil Engineering, Abadan Branch, Islamic Azad University, Abadan, Iran
E-Mail: Alireza.Bahrami@hig.se

ABSTRACT

This research is concerned with the dynamic behaviour of steel eccentrically braced frames (EBFs) having moment-shear link. The finite element software ABAQUS is used to analyse the EBFs. An experimentally tested EBF is modelled and the comparison of its obtained result with that of the experimental test validates the modelling method. An EBF is also designed having a moment-shear link. The designed EBF is modelled based on the verified modelling method. Then, the EBF is analysed under three selected earthquake records of Tabas, Chi-Chi, and Northridge. The lateral displacements, base shears, and energy dissipations of the EBF and also moment-shear link rotations are obtained from the results and compared. It is concluded that the largest to smallest values for the lateral displacement and base shear of the EBF, and also link rotation are all related to the Tabas, Chi-Chi, and Northridge records, respectively. However, the EBF dissipates the energy of the Tabas record more than the Northridge record, while, the latter is more than the Chi-Chi record.

Keywords: eccentrically braced frame, moment, shear, lateral displacement, base shear, energy dissipation, rotation.

1. INTRODUCTION

Steel moment frames can have stable inelastic and ductile behaviour under earthquakes, however, concentrically braced frames (CBFs) own higher lateral stiffness which can lead to the limitation of the damage due to drift. On the other hand, if braces buckle under earthquakes, the ductility and energy dissipation capacity of the CBFs can considerably deteriorate. EBFs combine the advantages of the moment frames and CBFs successfully, i.e., great ductility and lateral stiffness, during earthquakes.

The diagonal brace in the EBFs, at least at one end, is connected to the end of an isolated segment of beam that is referred to as link, rather than the beam-column connection. Links as structural fuses can dissipate earthquake input energy without degradation of strength and stiffness. They do it by limiting the forces that are transferred to the adjacent columns, braces, and beams [1].

The link length is of great importance in the design of the EBFs. The link can be either shear, moment, or moment-shear link based on its yielding behaviour. If the link yields in shear extending over its full length, it is a shear link, however, if the link yields in flexure at its ends, it is a moment link, whilst, if the link possesses the combination of shear and flexural yielding, it is a moment-shear link. Equation (1) determines the length range for the moment-shear link:

$$\frac{1.6\,M_p}{V_p} < e < \frac{2.6\,M_p}{V_p} \quad (1)$$

where e, M_p and V_p are the link length, nominal plastic moment strength, and nominal plastic shear strength of the steel section, respectively.

Considerable research has been undertaken on the behaviour of the EBFs since mid-1970's [2-14]. Nonetheless, this research evaluates the EBFs having moment-shear link under earthquake records.

The current research investigates the dynamic behaviour of the steel EBFs having moment-shear link. The finite element software ABAQUS is used for the analysis of the EBFs. An experimentally tested EBF is modelled in order to verify the modelling. All the features of the test are considered in the modelling. The modelling result is compared with the experimental test result and owing to their good agreement, the modelling accuracy is revealed. Then, an EBF is designed having a moment-shear link. Three earthquake records of Tabas, Chi-Chi, and Northridge are selected. The designed EBF is analysed subjected to the records. The lateral displacements, base shears, and energy dissipations of the frame and also moment-shear link rotations are examined and discussed.

2. VERIFICATION OF MODELLING

In order to verify the modelling of this research, an experimentally tested steel EBF with hollow rectangular cross-section [15] was modelled. The setup of the experimental test is illustrated in Figure-1. The overall height and width (L) of the test specimen were 3150 mm and 3660 mm, respectively. The column end support was pinned. A hydraulic actuator was used to transfer the horizontal force to a loading beam. The load was distributed to clevises equally at the top of each column by the loading beam. The steel of the link was A572 Gr. 50 having a nominal yield strength of 345 MPa. HSS 178 × 178 × 12.7 (US-7 × 7 × 1/2) and W 310 × 143 (US-12 × 96) were employed for braces and columns, respectively. The connections between beam, columns, and braces were moment resisting. The guidelines of ATC-24 [16] were applied for the loading protocol in the testing.

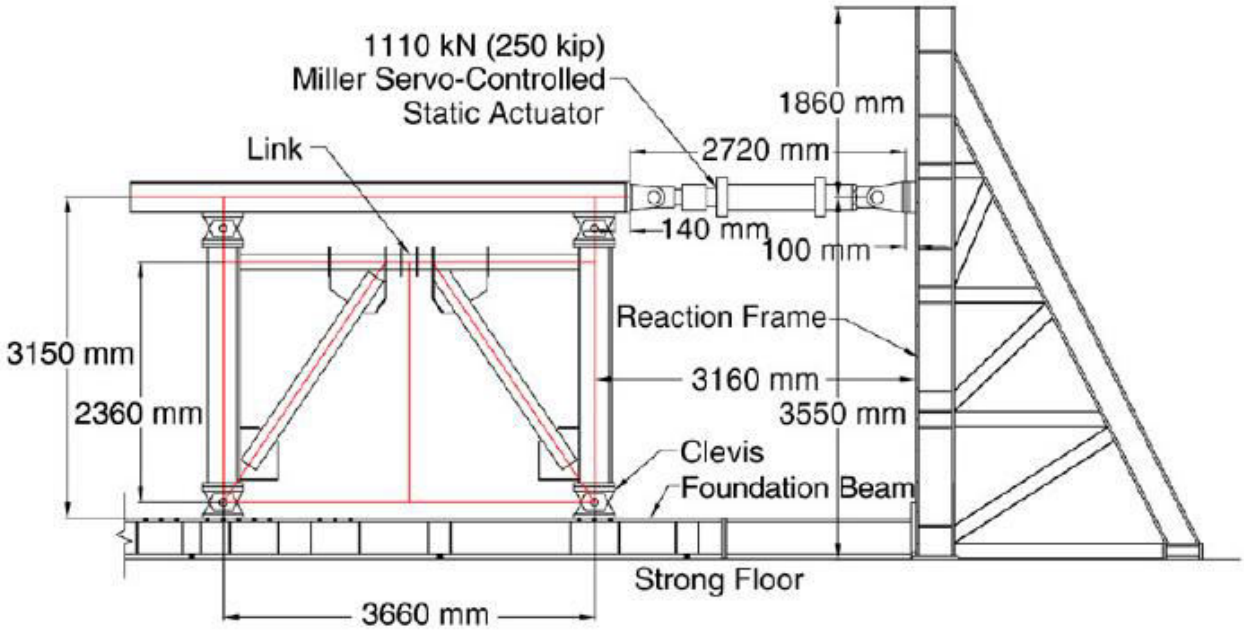

Figure-1. Setup of experimental test [15].

In the modelling, the features of the experimental test were exactly applied. The 4-node shell element S4R was used to model the specimen members. The material modelling was done as its vital part [17, 18]. A bilinear model with kinematic hardening behaviour was used for steel [19-21]. The same loading and boundary conditions as the test were considered in the modelling. The mesh size of 50 mm was considered as the most suitable mesh size for the modelling which was achieved from the conducted convergence study. This mesh size could lead to the exact result. Figure-2 demonstrates the typical meshing of the modelled EBF for the verification study.

In order to examine the obtained result from the modelling, it is compared with the test result. Accordingly, the link shear-link rotation diagram of the modelling is depicted based on the achieved results. Then, the diagram of this research (numerical) is compared with the experimental and finite element diagrams, as indicated in Figure-3. It can be observed from the figure that the diagrams agree well with each other which verifies the modelling. Consequently, the same modelling method is followed in the next stage for the analysis of the EBF.

3. DESIGN OF EBF HAVING MOMENT-SHEAR LINK

The EBF in this sections was similar to the verified EBF. However, the EBF was designed to have moment-shear link. According to the design, the link length was 750 mm and the first intermediate stiffener was placed 232 mm from the first stiffener.

4. ANALYSIS OF EBF HAVING MOMENT-SHEAR LINK

To analyse the designed EBF under the earthquake loads, three different earthquake records of Tabas, Chi-Chi, and Northridge were selected. Specifications of these records are listed in Table 1. In the table, M_w, PGA, PGV, and PGD are respectively as the magnitude of the earthquake, the peak ground acceleration, the peak ground velocity, and the peak ground displacement.

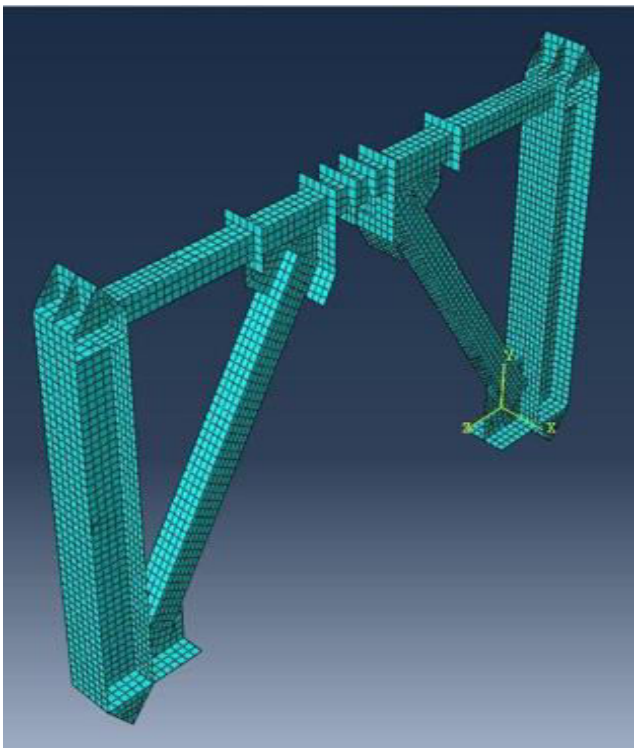

Figure-2. Typical meshing of modelled EBF for verification.

Table-1. Specifications of considered records [22].

Earthquake	M_w (Richter Scale)	PGA (g)	PGV (cm/s)	PGD (cm)
Northridge (1994)	6.70	0.349	32.25	9.30
Chi-Chi (1999)	7.70	0.89	98	15.85
Tabas (1978)	7.40	0.928	111.35	91.10

The designed EBF was modelled in ABAQUS on the basis of the verified modelling method described previously. Material specifications of the modelled EBF were similar to those of the verified EBF, too. On the other hand, the moment-shear link features explained in section 3 were adopted herein. The Tabas, Chi-Chi, and Northridge earthquake records (Table-1) were applied to the frame. Figure-4 shows the modelled EBF having the moment-shear link.

5. RESULTS AND DISCUSSIONS

The results of the further analyses on the EBF are presented and discussed below.

5.1 Lateral Displacements of EBF having Moment-Shear Link

Figures-5-7 illustrate the lateral displacements diagrams obtained from the analyses of the EBF subjected to the earthquake records of Tabas, Chi-Chi, and Northridge. The maximum lateral displacements of the EBF are 4.17 cm, 3.38 cm, and 2.63 cm respectively under the records of Tabas, Chi-Chi, and Northridge (Figure-8). Consequently, the lateral displacement of the EBF subjected to the Tabas record is 23.4% and 58.6% larger than the lateral displacements of the EBF under the Chi-Chi and Northridge records, respectively. These displacements are directly related to the peak ground accelerations of the records. In addition, the EBF has become unstable at the times of 10.75 seconds, 7.50 seconds, and 3.70 seconds respectively under the records of Tabas, Chi-Chi, and Northridge. These unstable times can be witnessed as an instantaneous displacement jump in the diagrams.

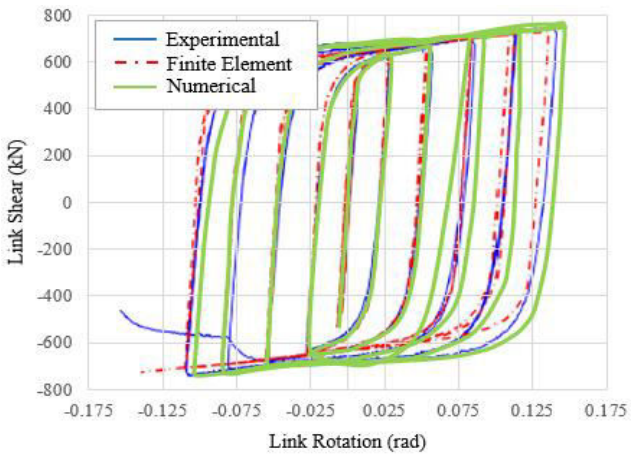

Figure-3. Verification of modelling.

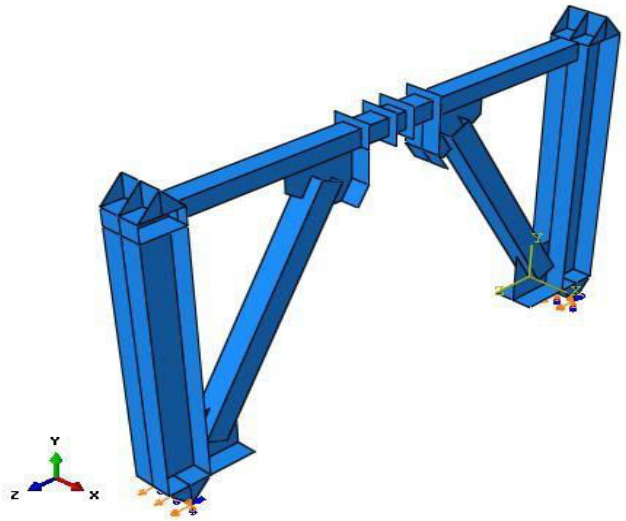

Figure-4. Modelled EBF having moment-shear link.

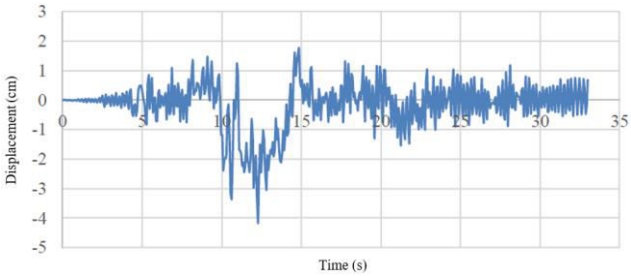

Figure-5. Lateral displacement of EBF having moment-shear link subjected to Tabas record.

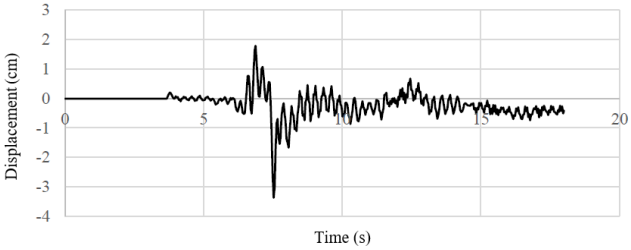

Figure-6. Lateral displacement of EBF having moment-shear link subjected to Chi-Chi record.

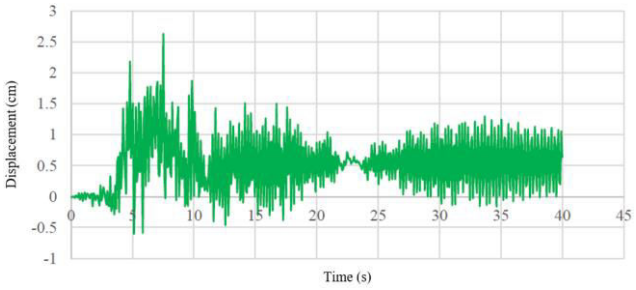

Figure-7. Lateral displacement of EBF having moment-shear link subjected to Northridge record.

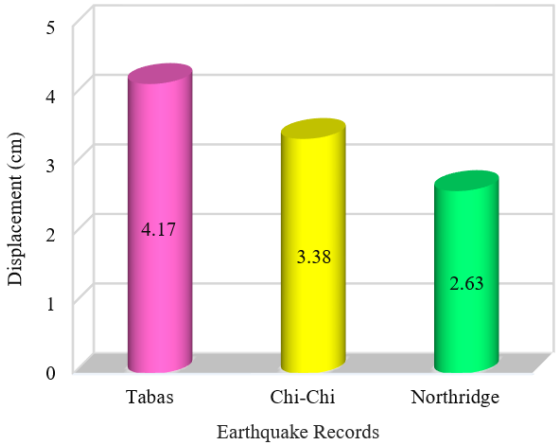

Figure-8. Comparison of lateral displacements of EBF having moment-shear link subjected to different records.

5.2 Base Shears of EBF having Moment-Shear Link

The base shears of the EBF under the earthquake records were obtained and their diagrams are elaborated in Figures-9-11. Also, the maximum base shears of the EBF under the records are displayed in Figure-12. The maximum base shear of 4620 kN was achieved for the EBF subjected to the Tabas record. However, the base shears of 4218 kN and 3045 kN were resulted for the EBF under the Chi-Chi and Northridge records, respectively. Therefore, the base shear of the EBF subjected to the Tabas record is 9.5% greater than that of the EBF under the Chi-Chi record, while, the latter is 38.5% larger than that under the Northridge record. This is because of the point that the base shear is dependent on the acceleration and the acceleration of the Tabas record is higher than the Chi-Chi and Northridge records, respectively.

5.3 Energy Dissipations of EBF having Moment-Shear Link

Figures-13-15 demonstrate the achieved energy dissipations diagrams of the EBF under the records. The energy dissipations of the EBF subjected to the Tabas and Chi-Chi records are zero during about the first 7 seconds, whilst, the energy dissipation is zero during the first 4 seconds for the Northridge record. Then, the developments of the energy dissipations of the EBF were started. However, the energy dissipation of the EBF under the Chi-Chi record started developing with a steeper slope compared with the energy dissipations under the Tabas and Northridge records. The energy dissipations of the EBF subjected to the Tabas, Chi-Chi, and Northridge records were lasted for 32.5 seconds, 17.5 seconds, and 40 seconds, respectively.

Furthermore, the maximum energy dissipations are indicated in Figure-16. The maximum energy dissipations of the EBF under the Tabas, Chi-Chi, and Northridge records are 72010 kN-cm, 2717 kN-cm, and 21100 kN-cm, respectively. Less energy dissipation of the EBF subjected to the Chi-Chi record than the energy dissipations of the EBF under the Tabas and Northridge records is due to much steeper slope of the energy dissipation diagram of the Chi-Chi record than the Tabas and Northridge records.

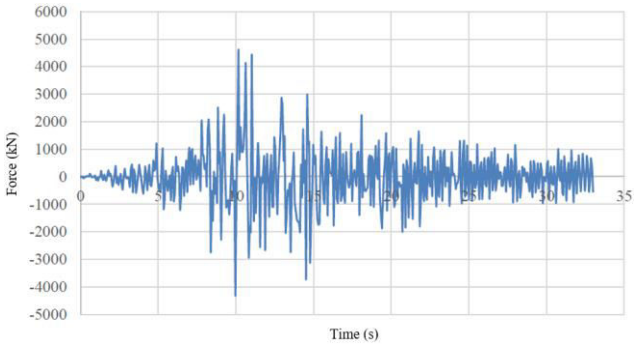

Figure-9. Base shear of EBF having moment-shear link subjected to Tabas record.

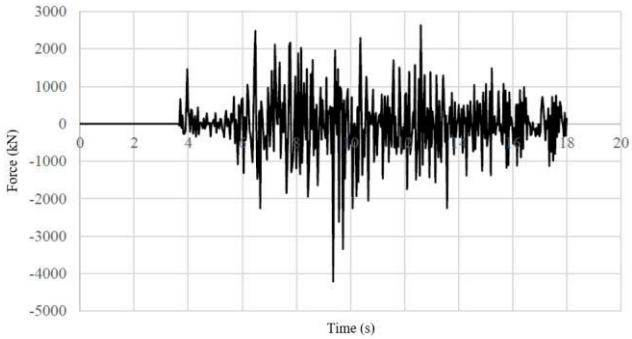

Figure-10. Base shear of EBF having moment-shear link subjected to Chi-Chi record.

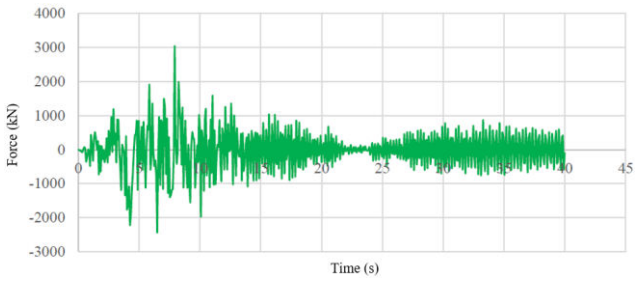

Figure-11. Base shear of EBF having moment-shear link subjected to Northridge record.

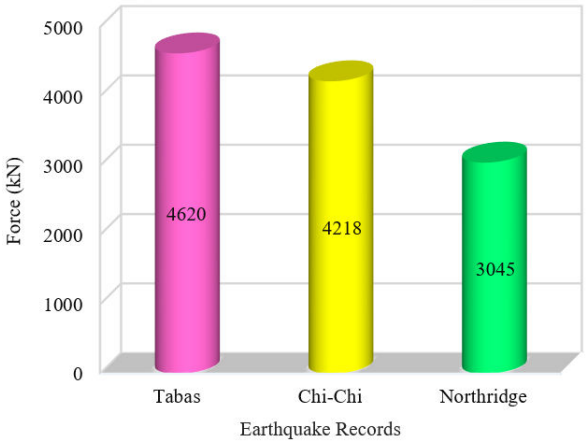

Figure-12. Comparison of base shears of EBF having moment-shear link subjected to different records.

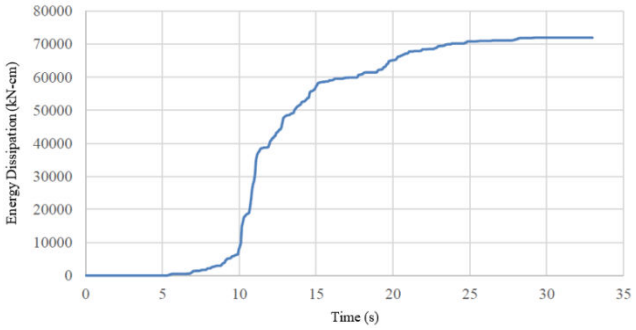

Figure-13. Energy dissipation of EBF having moment-shear link subjected to Tabas record.

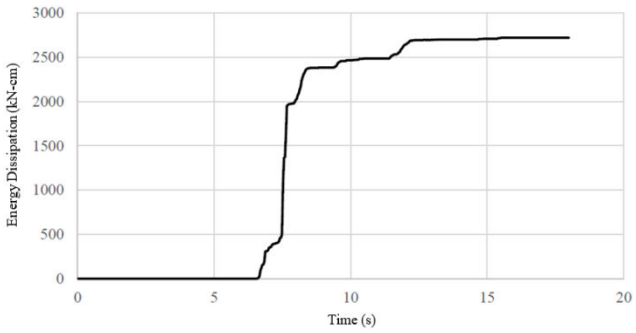

Figure-14. Energy dissipation of EBF having moment-shear link subjected to Chi-Chi record.

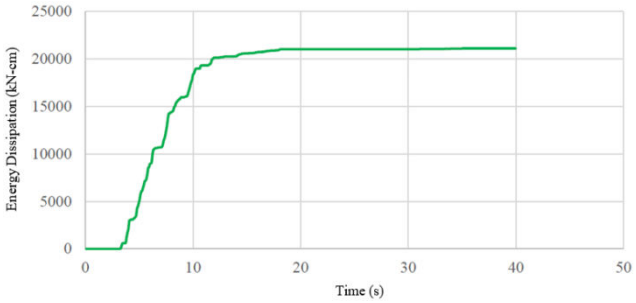

Figure-15. Energy dissipation of EBF having moment-shear link subjected to Northridge record.

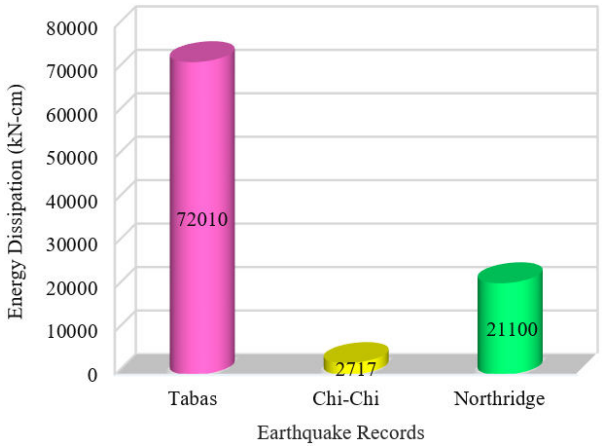

Figure-16. Comparison of energy dissipations of EBF having moment-shear link subjected to different records.

5.4 Rotations of Moment-Shear Link of EBF

The rotations of the moment-shear link of the EBF under the earthquake records were obtained and compared in Figure-17. According to the figure, the rotations of the link are 9.4 rad, 7.6 rad, and 5.9 rad, respectively for the EBF under the Tabas, Chi-Chi, and Northridge records. This figure indicates 23.7% larger rotation of the EBF under the Tabas record than the Chi-Chi record, while, the latter is 28.8% greater than the rotation of the EBF subjected to the Northridge record because the link rotation is directly proportional to the lateral displacement. As it was mentioned in section 5.1, the Tabas earthquake causes the largest lateral displacement (4.17 cm) of the EBF which leads to the highest rotation as 9.4 rad.

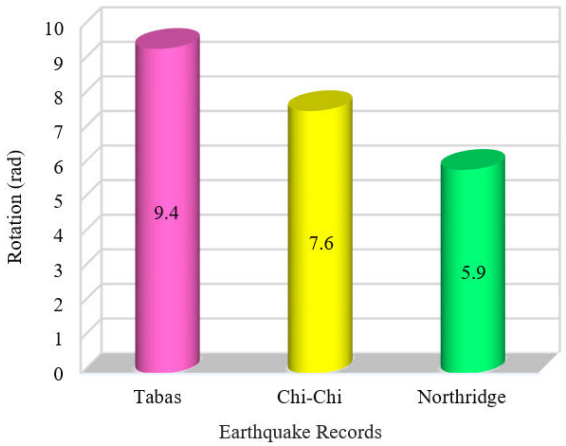

Figure-17. Comparison of rotations of moment-shear link of EBF subjected to different records.

5.5 Failure Mode of EBF

Failure mode of the studied EBF under the records is mainly buckling of the brace and/or large rotation of the link. Figure-18 presents the failure mode of the EBF subjected to the Chi-Chi record. As it can be seen from the figure, buckling of the brace, rotation of the link, and local buckling of the column flange have occurred in the EBF which are also shown in the figure.

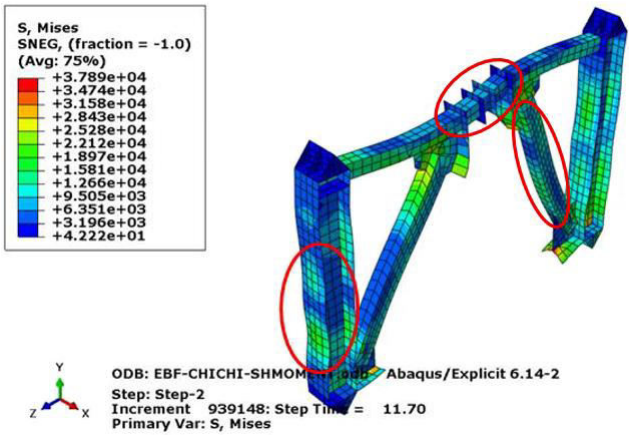

Figure-18. Failure mode of EBF subjected to Chi-Chi record.

6. CONCLUSIONS

This research assessed the dynamic behaviour of EBFs having moment-shear link. The modelling and analysis of the EBFs were done using ABAQUS. The modelling was validated by the comparison of its result with that of the experimental test. An EBF was also designed having a moment-shear link. Since the modelling was validated, the designed EBF was modelled following the modelling method. Then, three earthquake records of Tabas, Chi-Chi, and Northridge were selected for the analysis of the EBF. The lateral displacements, base shears, and energy dissipations of the EBF and also moment-shear link rotations were achieved from the results and compared. It was found that the hierarchy of the records from the viewpoint of causing the largest to smallest values for the lateral displacement and base shear of the EBF, and link rotation was the Tabas, Chi-Chi, and Northridge records. Nonetheless, the energy dissipation of the EBF was greater under the Tabas record than the Northridge record, whilst, the latter was larger than the Chi-Chi record.

REFERENCES

[1] S-H Chao and S. C. Goel. 2005. Performance-based seismic design of EBF using target drift and yield mechanism as performance criteria. Department of Civil and Environmental Engineering. The University of Michigan. Ann Arbor. MI 48109-2125.

[2] C. W. Roeder and E. P. Popov. 1978. Eccentrically braced steel frames for earthquakes. Journal of the Structural Division. 104(3): 391-412.

[3] M. D. Engelhardt and E. P. Popov. 1992. Experimental performance of long links in eccentrically braced frames. Journal of Structural Engineering. 118(11): 3067-3088.

[4] A. Jain, S. Koboevic and R. Redwood. 1996. Design and behaviour of eccentrically braced frames with flexural links. Advances in Steel Structures. Proceedings of International Conference on Advances in Steel Structures. Hong Kong. 233-237.

[5] T. Okazaki, G. Arce, H-C Ryu and M. D. Engelhardt. 2005. Experimental study of local buckling, overstrength, and fracture of links in eccentrically braced frames. Journal of Structural Engineering. 131(10): 1526-1535.

[6] M. Bosco and P. P. Rossi. 2009. Seismic behaviour of eccentrically braced frames. Engineering Structures. 31(3): 664-674.

[7] M. Ohsaki and T. Nakajima. 2012. Optimization of link member of eccentrically braced frames for maximum energy dissipation. Journal of Constructional Steel Research. 75: 38-44.

[8] G. Yiğitsoy, C. Topkaya and T. Okazaki. 2014. Stability of beams in steel eccentrically braced frames. Journal of Constructional Steel Research. 96: 14-25.

[9] K. Young and H. Adeli. 2016. Fundamental period of irregular eccentrically braced tall steel frame structures. Journal of Constructional Steel Research. 120: 199-205.

[10] M. Bosco, E. M. Marino and P. P. Rossi. 2017. A design procedure for dual eccentrically braced-moment resisting frames in the framework of Eurocode 8. Engineering Structures. 130: 198-215.

[11] J. Ruiz-García, E. Bojorquez and E. Corona. 2018. Seismic behavior of steel eccentrically braced frames under soft-soil seismic sequences. Soil Dynamics and Earthquake Engineering. 115: 119-128.

[12] E. Tapia-Hernández and S. García-Carrera. 2019. Inelastic response of ductile eccentrically braced frames. Journal of Building Engineering. 26: Article number 100903.

[13] Z. Yao, W. Wang, C. Fang and Z. Zhang. 2020. An experimental study on eccentrically braced beam-through steel frames with replaceable shear links. Engineering Structures. 206: Article number 110185.

[14] A. Bahrami and M. Heidari. 2020. Dynamic analysis of steel eccentrically braced frames with shear link.

International Journal of Engineering Research and Technology. 13(2): 233-239.

[15] J. W. Berman and M. Bruneau. 2007. Experimental and analytical investigation of tubular links for eccentrically braced frames. Engineering Structures. 29: 1929-1938.

[16] ATC. Guidelines for cyclic seismic testing of components of steel structures. Report-24. 1992. Applied Technology Council.

[17] A. Bahrami, W. H. Wan Badaruzzaman and S. A. Osman. 2013. Performance of axially loaded tapered concrete-filled steel composite slender columns. Journal of Civil Engineering and Management. 19(5): 705-717.

[18] A. Bahrami and S. Matinrad. 2019. Blast effects on reinforced concrete connections. International Journal of Scientific and Technology Research. 8(11): 3604-3610.

[19] A. Bahrami and M. Yavari. 2019. Hysteretic assessment of steel-concrete composite shear walls. International Journal of Recent Technology and Engineering. 8(2): 5640-5645.

[20] A. Bahrami and S. Matinrad. 2019. Response of steel beam-to-column bolted connections to blast loading. International Journal of Recent Technology and Engineering. 8(3): 3639-3648.

[21] A. Bahrami and S. Matinrad. 2020. Resistance of blast-loaded steel and reinforced concrete beam-to-column connections. International Journal of Engineering Research and Technology. 13(1): 12-27.

[22] http://ngawest2.berkeley.edu/.